Supporting Information for

Unprecedented high selectivity of *n*-hexane dehydroaromatization to benzene over metal-free phosphorus-doped activated carbon catalysts

Yong Li[a,b], Shuhao Bao[a,b], Hong Zhao[b*], Bing Feng[b], Siyuan Chen[b], Tangjie Gu[c], Bo Yang[c*], Biao Jiang[b*]

[a] College of Sciences, Shanghai University, Shanghai 200444, China
[b] Green Chemical Engineering Technology Research Center, Shanghai Advanced Research Institute, Chinese Academy of Sciences, Shanghai 201210, China,
[c] School of Physical Science and Technology, Shanghai Tech University, 393 Middle Huaxia Road, Shanghai 201210, China
zhaoh@sari.ac.cn, jiangb@sari.ac.cn, yangbo1@shanghaitech.edu.cn

1. Experimental details

(1) Catalyst preparation

All chemicals were purchased from Sinopharm Chemical Reagent Co. Ltd. and used as received without further purification: phosphoric acid (H_3PO_4, 85 wt.%, AR), H_2O_2 (30 wt.%, AR), HF (40 wt.%, AR). Before use, H_2O_2 was diluted to 15 wt.% and HF was diluted to 14 wt.% with deionized water. Deionized water was used in the procedures when applicable. Coconut shell based activated carbon with a particle size of about 2 mm was purchased from Ningxia Guanghua Activated Carbon Co., Ltd. Prior to the P-doping treatment, the activated carbon sample was first soaked in 14 wt.% aqueous HF solution at 70 °C for 4 hours. After HF removal by filtration, washing and drying at 105 °C overnight, the obtained solids were soaked in 15 wt.% aqueous H_2O_2 solution at 80 °C for 6 hours. After filtration, washing and drying at 105 °C overnight, the obtained solids were then denoted as AC. The P-doping procedure was carried as follows: Different amounts of 85 wt.% H_3PO_4 solution were added to deionized water obtaining a series of H_3PO_4 solutions in the concentration range of 1~15 wt.%. Typically, 60 mL H_3PO_4 solution was added to 20 g AC under stirring to ensure a uniform mixture, which was transferred into an autoclave and heated at 180 °C for 6 hours as the hydrothermal treatment. The obtained solids were filtrated, washed with deionized water and dried at 80 °C for 6 hours. For catalytic performance evaluation, the dried samples were loaded in the quartz tube reactor and activated in situ under an He flow at 750 °C for 2 hours with a ramping rate of 2 °C min^{-1} and He flow rate of 40 mL·min^{-1}. Subsequently, the catalyst bed was purged with a N_2 gas flow (40 mL min^{-1}) at 550 °C for 30 min. After that, the dehydroaromatization reaction tests were performed. For characterization investigations, the dried samples were loaded in the quartz tube reactor and treated under an He flow at 750 °C for 2 hours with a ramping rate of 2 °C min^{-1} and He flow rate of 40 mL min^{-1} to obtain the P-doped activated carbon samples denoted as P@AC-x, where x was the P amount introduced as detected by XPS analysis.

HZSM-5 zeolite with a Si to Al ratio of 34.1 was obtained from Nankai University Catalyst Co. Ltd. The P-modified HZSM-5 catalyst was prepared by impregnation of

HZSM-5 with an aqueous solution of H_3PO_4 applying an incipient wetness technique [1]. The resulting material was dried at 105 °C overnight and calcined at 550 °C for 5 hours with a ramping rate of 2 °C min^{-1} to obtain the final P/HZSM-5 catalyst. In this work, the P amount was 1.71 wt.% and the ratio of Si to Al was 35.8 in the P/HZSM-5 sample.

(2) Catalytic reaction tests

The dehydroaromatization performances of the samples were evaluated at atmospheric pressure in a continuous flow fixed-bed reactor equipped with a quartz tube of 600 mm length and 10 mm inner diameter. The catalyst was loaded in the quartz tube reactor and activated *in situ* under He flow. The residual space in the quartz tube reactor was also filled with quartz sand to minimize the contribution of the thermal reaction. The reaction temperature was regulated by an automatic temperature controller manufactured by Y-Feng Shanghai Co. Ltd. The flow rate of *n*-hexane feed and N_2 carrier gas were precisely regulated by a 2ZB-1L10 piston pump (Beijing Xingda Science & Technology development Co. Ltd.) and a mass flowmeter (Beijing Seven Star Co. Ltd.), respectively. The evaluation conditions were as follows: catalyst loading of 1.0 g, reaction temperature of 550 °C, atmospheric reaction pressure, N_2 carrier gas flow rate of 40 mL min^{-1}, *n*-hexane model feed flow rate of 1.0 mL h^{-1} with a calculated WHSV of 0.67 h^{-1}.

The products were periodically analyzed online by gas chromatography (Agilent 7890B) equipped with a thermal conductivity detector (TCD) and a flame ionization detector (FID). A GS-GASPRO capillary column (30 m × 0.32 mm) were connected to FID for hydrocarbon analysis, while Porapak Q (80-100 mess) columns were connected to TCD for H_2 analysis.

Hexane conversion as well as the selectivity to the organic products was calculated based on the carbon numbers by area normalization method:

$$Con_{hexane} = \left(1 - \frac{A_{hexane}}{A_{total}}\right) \times 100\%$$

where A_{hexane} was the *n*-hexane peak area, and A_{total} was the total peak area of both hexane and hydrocarbon products at the outlet. The selectivity was calculated by

comparing the corresponding peak areas A_i to sum of all product peak areas:

$$Sel_i = \frac{A_i}{\sum A_i} \times 100\%$$

H_2 was analyzed by TCD, and the molar concentration in the outlet gas was calculated according to:

$$C_{H_2} = A_{H_2} * f_{H_2}$$

where A_{H2} was the H_2 peak area and f_{H2} was absolute correction factor.

(3) Catalyst Characterization

XRD images were procured using a Rigaku Mini Flex 600 X-ray diffractometer with the Cu Kα radiation at 40kV and 15mA with scanning rate of 2°/min. The morphology of the carbon samples was examined by transmission electron microscopy (TEM) micrographs taken by a JEM 2010 electron microscope operated at an accelerating voltage between 80 and 200 kV. Fourier transform infrared spectroscopy (FT-IR) was performed on a Perkin Elmer Spectrum Two FT-IR spectrometer equipped with an attenuated total reflection (ATR) unit. Raman spectra were collected using a Renishaw in Via unit with an Ar ion laser (Wavelength = 532nm). The textural data of the samples were determined by measuring N_2 isotherm at 77K with a Micromeritics ASAP 2020 automated system. The pore size distribution (PSD) was determined by the desorption branch of the data of N_2 adsorption-desorption. The total surface area was calculated according to the Brunauer-Emmet-Teller (BET) isothermal equation. The microporous volume, mesoporous volume, and external surface area were evaluated by the t-plot method. Temperature-programmed-desorption of NH_3 (NH_3-TPD) was performed on a Micromeritics ASAP 2920 with a thermal conductivity detector (TCD). The catalyst was first pretreated in a He flow at 953 K for 1.5 hours. After cooling down to 373 K under He flow, the sample was exposed to 15 % NH_3/He at 373 K. Then the sample was swept by He at 323 K for 1 hour. Subsequently, signals were recorded while the temperature was increased from 323 to 1073 K at a heating rate of 10 K/min. The X-ray photoelectron spectroscopy (XPS) investigations were conducted with a ESCALAB

250 spectrometer from Thermo Fisher Scientific using Al Kα radiation with an Al Kα (1486.6 eV, 15 mA) X-ray source. For those experiments, C 1s, P 2p, and O 1s bands were recorded. The C 1s peak at 284.6 eV was used to correct charging effects. Shirley backgrounds were subtracted from the raw data to obtain the areas of the C 1s peak.

2. Density Functional Theory (DFT) Calculations

All DFT calculations were performed with the Vienna ab initio simulation package (VASP).[2-4] The projector-augmented wave (PAW) pseudopotentials were used to describe the ion core and its interaction with valence electrons.[5,6] The Perdew Burke Ernzerhof (PBE) functional was used in all geometry optimizations,[7] and energy cutoff was set to 500 eV. All atoms in the model were relaxed and optimized using a force-based conjugate-gradient algorithm until the force was smaller than 0.05 eV/Å. A $2\times2\times1$ Monkhorst-Pack k-point grid was used under consideration of spin polarization in the calculations. The core-level binding energy shifts (CLS) were calculated using the method reported in the literature.[8]

The XPS and FT-IR analysis results shown above indicated that (i) the O/P atom ratio is 3.32 (see Table S2); (ii) both C-O-P and C-P-O stretching vibrations can be identified in P@AC; (iii) peaks relating to P=O and P-OH vibrations can be found in P@AC. Therefore, assuming that P atoms would bind with a maximum of three O atoms, we compared the stability of possible structures of the catalyst, including PO_3 and $P(O)_2(OH)$, with C-P and C-O binding to the surface. Considering that some of the oxygen atoms might be at the edge sites of AC and the number of O atoms binding with P might be less than three, we also calculated the stability of $C_2-P(O)(OH)$ and $(CO)_2-P(O)(OH)$ on the surface.

The formation energy (E_{form}) of the possible catalyst structures were calculated with the following equation:

$$E_{form} = E_{(CaHcPO3)} + 0.5 \times (b-c+1) \times E_{(H2)} + E_{(H2O)} - E_{(CaHb)} - E_{(H3PO4)}$$

where $E_{(CaHcPO3)}$ and $E_{(CaHb)}$ are the energies of P@ACs and pristine carbon materials, respectively, and $E_{(H2)}$, $E_{(H2O)}$, and $E_{(H3PO4)}$ are the energies of gaseous H_2, H_2O, and H_3PO_4, respectively, under consideration of the mass balance. The calculated E_{form} and

the corresponding configurations are presented in Fig. 3 and Fig. S6.

3. *List of Figures and Tables*

Fig. S1 (a) the product selectivity over P@AC-0.35 (a) and HZSM-5 (b).

Fig. S2 (a) the XRD spectra, (b) Raman spectra and (c) the DFT pore distribution of AC and P@AC

samples and (d) the XRD spectra of HZSM-5 and P/HZSM-5.

Fig. S3 The high-resolution electron micrograph of P@AC-1.68.

the XRD spectra of HZSM-5 and P/HZSM-5.

Fig. S4 (a) The XPS spectrum survey of P@AC-1.68, (b) the high resolution XPS C 1s spectra of

P@AC-1.68, (c) The XPS spectrum survey of P@AC-0.35, and the high resolution XPS C 1s spectra

(d), P 2p spectra (e) and O 1s spectra (f) of P@AC-0.35.

Fig. S5 (a) The XPS spectrum survey of P/HZSM-5, (b) the high resolution XPS P 2p spectra of

P/HZSM-5.

Fig. S6 Side views of the optimized structures of potential catalysts.

Fig.S7 A stability test of P@AC-1.68.

Scheme S1 The proposed structural distribution of P on P/HZSM-5 and P@AC.

Table S1 Textural properties of P free AC and P@AC samples.

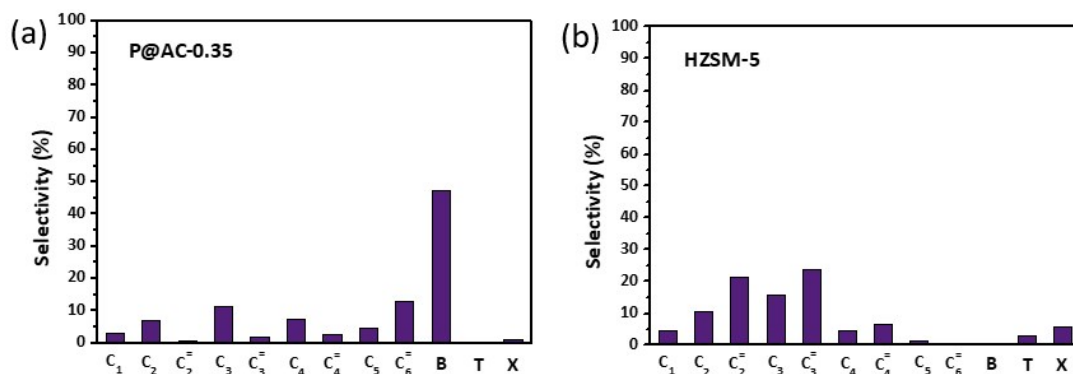**Table S2** Element compositions of AC and P@AC samples from XPS.

Fig.s1 (a) The product selectivity over P@AC-0.35 (a) and HZSM-5 (b). Reactions were conducted at 550 °C, the catalyst loading is 1.0 g, N_2 flow rate is 40 mL min^{-1} and the model feed of n-hexane is 1.0 mL h^{-1}. Note that the reaction data in Fig. S1 (a) are obtained after reaction for 10 min.
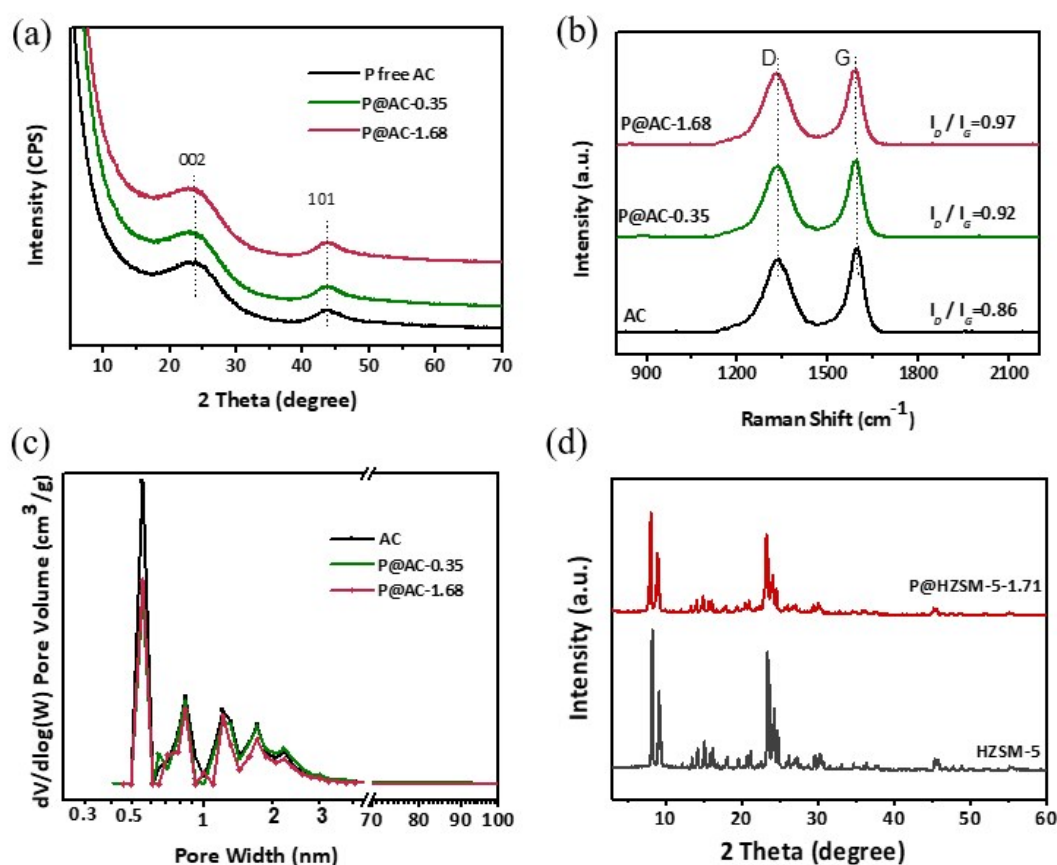

Fig.S2 The XRD spectra (a), Raman spectra (b) and the DFT pore distribution (c) of AC and P@AC samples. (d) the XRD spectra of HZSM-5 and P/HZSM-5.
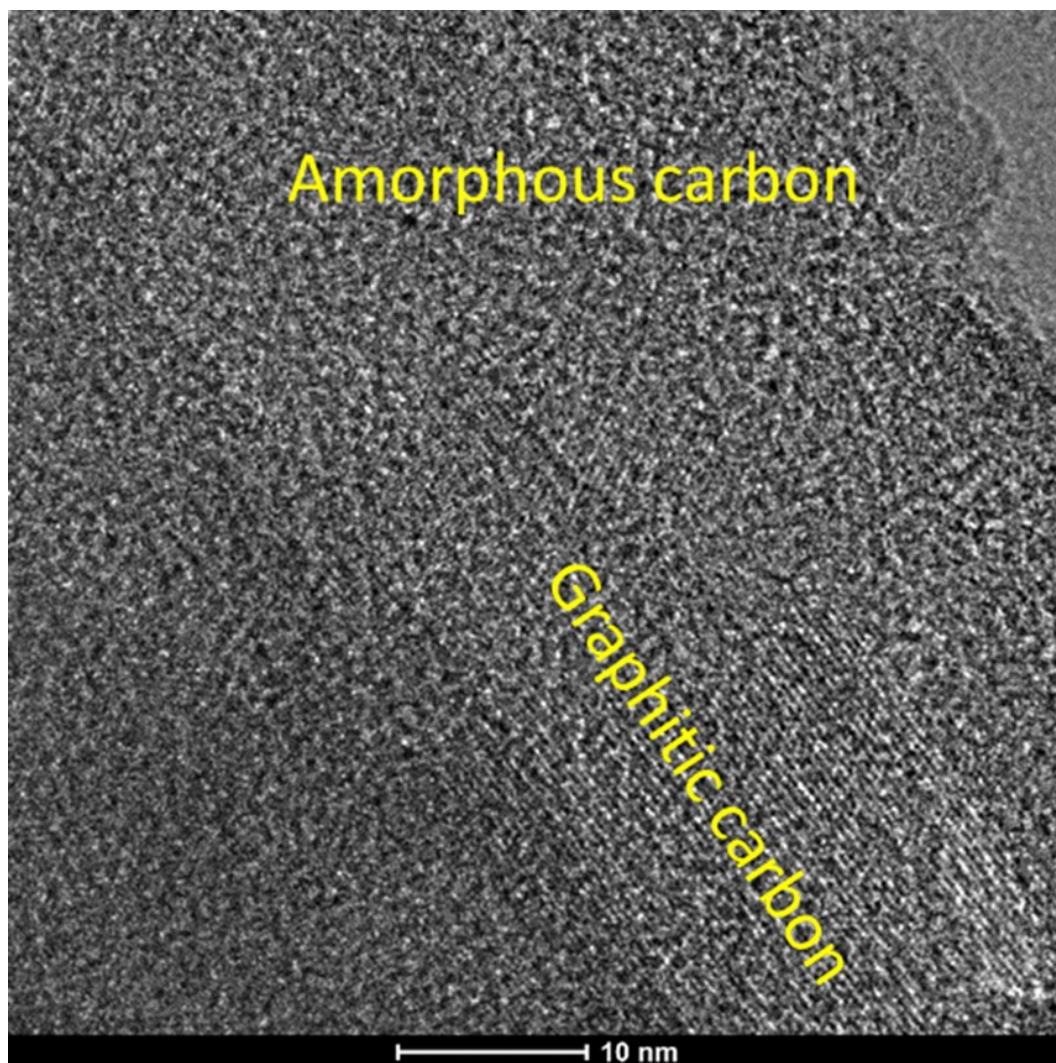
Fig.S3 The high-resolution electron micrograph of P@AC-1.68
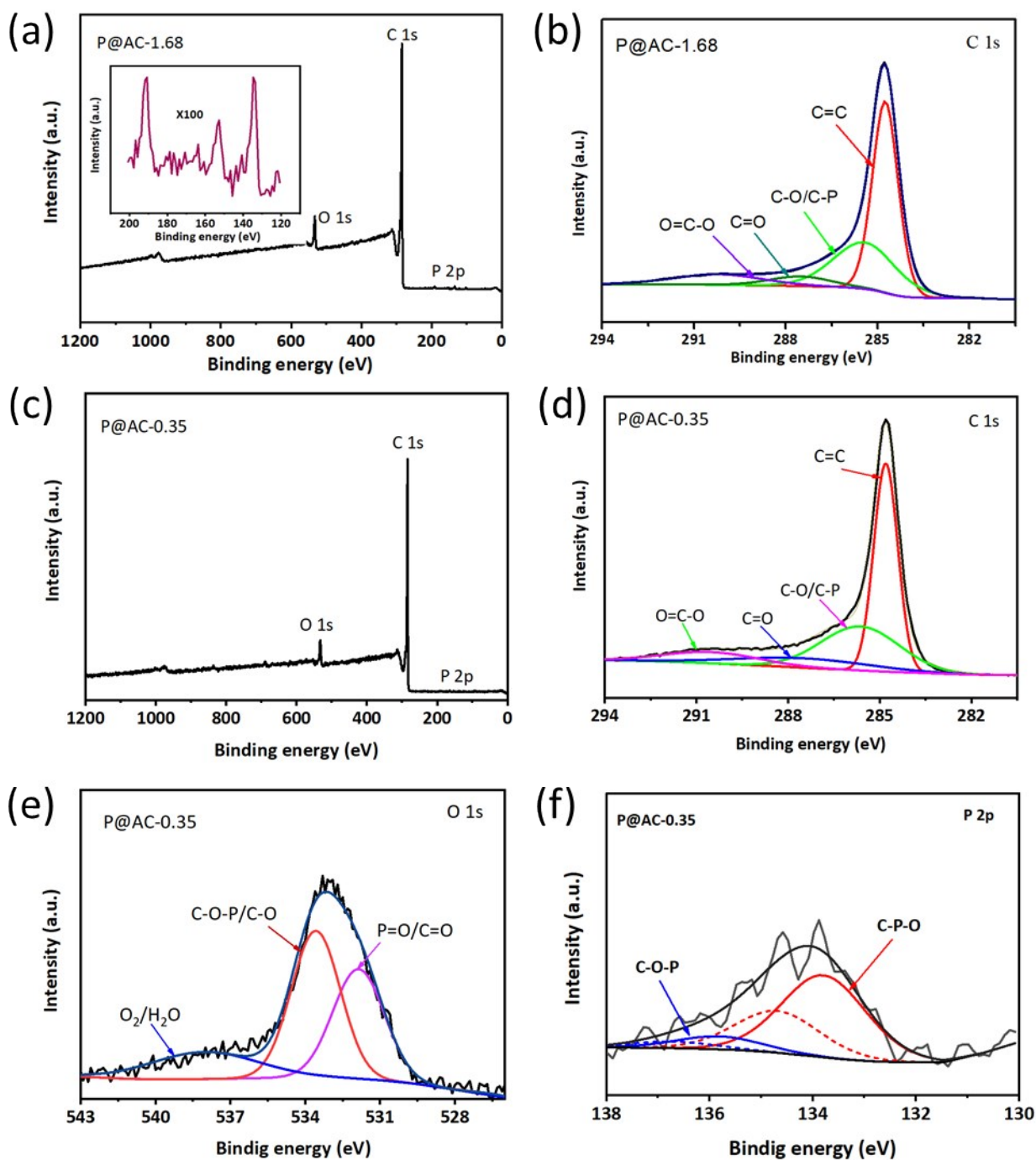
Fig. s4 (a) The XPS spectrum survey of P@AC-1.68, (b) the high resolution XPS C 1s spectra of P@AC-1.68, (c) The XPS spectrum survey of P@AC-0.35, and the high resolution XPS C 1s spectra (d), P 2p spectra (e) and O 1s spectra (f) of P@AC-0.35.
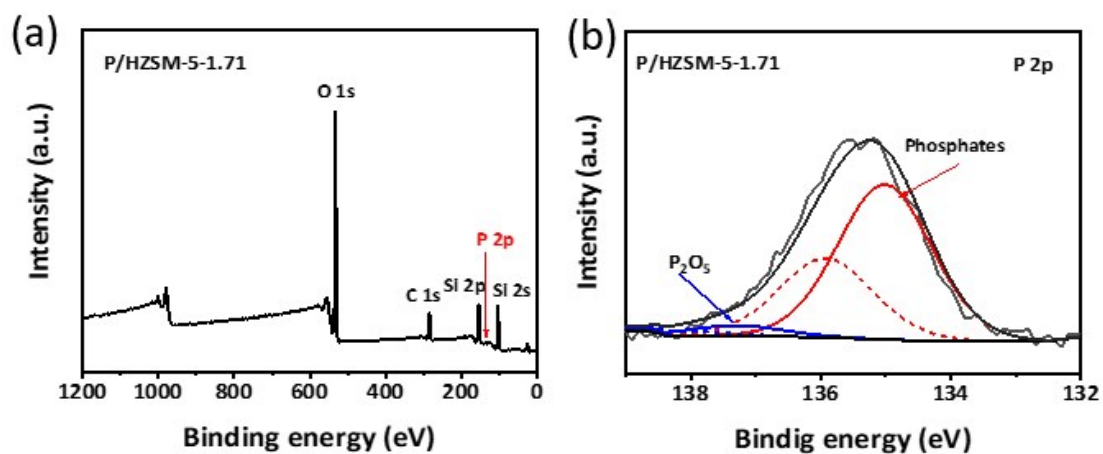
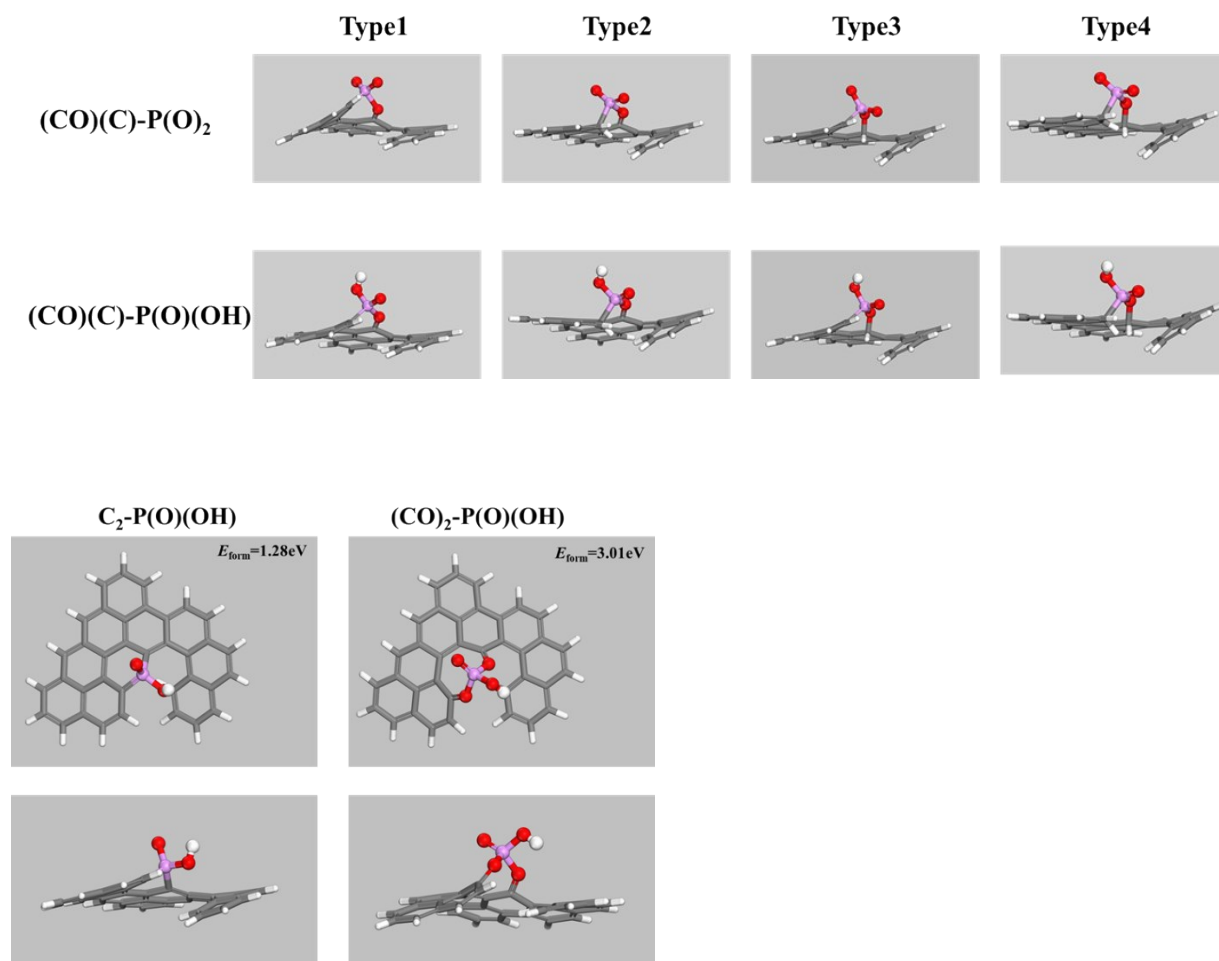**Fig. S5** (a) The XPS spectrum survey and (b) the high resolution XPS O 1s spectra of

P/HZSM-5-1.71.

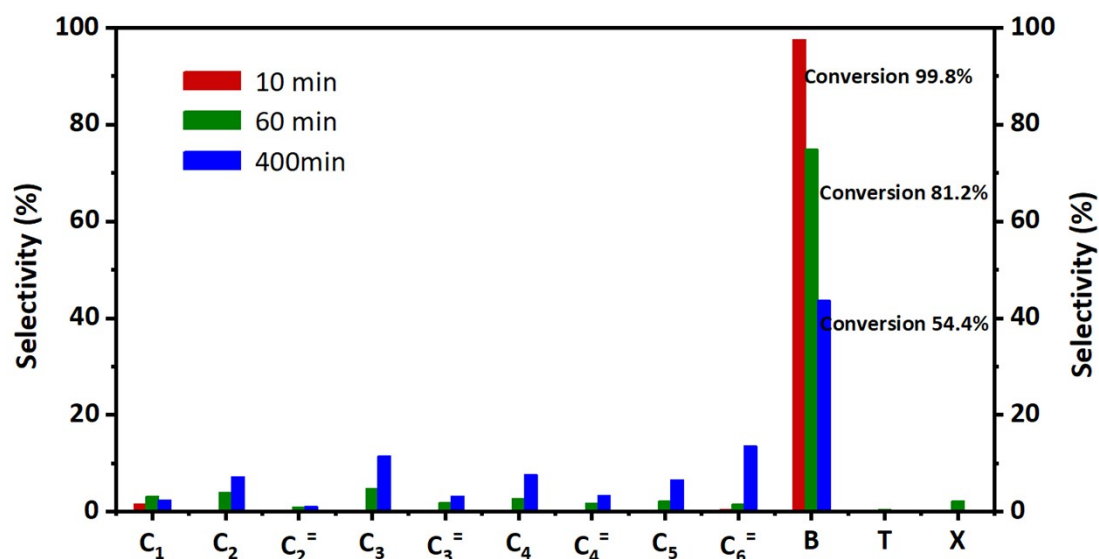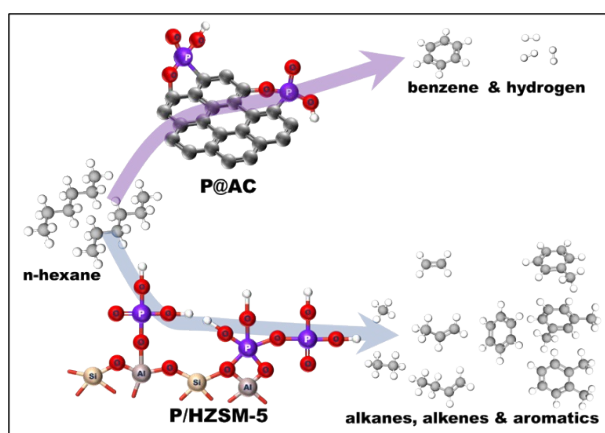**Fig. S6** Side views of the optimized structures of potential catalysts

Fig.S7 A stability test of P@AC-1.68. Reactions were conducted at 550 °C, the catalyst loading is 1.0 g, N_2 flow rate is 40 mL min^{-1} and a model feed of n-hexane is 1.0 mL h^{-1}.

Scheme S1 The proposed structural distribution of P on P/HZSM-5 and P@AC.

Table S1 Textural properties of P free AC and P@AC samples

Sample	S_{BET} m^2·g^{-1}	S_{micro} m^2·g^{-1}	S_{ext} m^2·g^{-1}	V_{total} cm^3·g^{-1}	V_{micro} cm^3·g^{-1}	D_{DFT} nm	P%
AC	1278.6	1039.7	238.8	0.55	0.43	0.60	-
P@AC-0.35	1251.7	970.4	281.3	0.52	0.40	0.60	0.35
P@AC-1.68	1060.4	827.2	233.2	0.49	0.38	0.58	1.68

samples	C %	O %	P %	O/P %
AC	96.13	3.87	0	-
P@AC-0.35	93.60	6.05	0.35	17.29
P@AC-1.68	92.84	5.58	1.68	3.32

Table S2 Element compositions of AC and P@AC samples from XPS

Reference

1   T. Blasco, A. Corma, and J. Martínez-Triguero, *J. Catal.* 2006, **237**, 267-277.
2   G. Kresse and J. Furthmuller, *Phys. Rev. B*, 1996, **54**, 11169-11186.
3   G. Kresse and J. Furthmuller, *Comput. Mater. Sci*, 1996, **6**, 15-50.
4   G. Kresse and J. Hafner, *Phys. Rev. B*, 1993, **47**, 558-561.
5   G. Kresse and D. Joubert, *Phys. Rev. B*, 1999, **59**, 1758-1775.
6   P. E. Blöchl, *Phys. Rev. B*, 1994, **50**, 17953-17979.
7   J. P. Perdew, K. Burke and M. Ernzerhof, *Phys. Rev. Lett.*, 1996, **77**, 3865-3868.
8   Z. Zeng, X. Ma, W. Ding and W. Li, *Sci. China Chem.*, 2010, **53**, 402-410.